Electronic Supplementary Material (ESI) for ChemComm.
This journal is © The Royal Society of Chemistry 2025

Supplementary Information

Interfacial Molecular Layer Induced by Trace Chlorogenic Acid for Highly Stable Zinc Anode

Jinlong Zhang,[†] Bing Cai,[†] Qing Wu, Jun Huang[*]

Department of Polymeric Materials & Engineering, College of Materials & Metallurgy, Guizhou University, Huaxi District, Guiyang 550025, P. R. China.

E-mail: huangj@gzu.edu.cn

[†] These authors contributed equally.

Experimental Section

1) Chemicals and materials

Chlorogenic acid (CGA, AR grade, 98%), zinc sulfate ($ZnSO_4 \cdot 7H_2O$, 99.995%), ammonium acetate (CH_3COONH_4, AR grade), and manganese acetate ($(CH_3COO)_2Mn$, 98%) were purchased from Aladdin. Zine foil (thickness of 100 μm, 99.99%), copper foil (thickness of 90 μm), carbon cloth, and coin cells (CR2032) were all purchased from the Canrd company. Glass fiber separator (thickness of 0.29 mm, GF-A) was purchased from Olegee technology.

2) Preparation of the electrolytes

The 1 M $ZnSO_4$ was prepared by dissolving 2.8756 g $ZnSO_4 \cdot 7H_2O$ into 10.0 mL deionized water. Different amounts (0.25 ~ 4.0 wt% of 2.8756 g $ZnSO_4 \cdot 7H_2O$, 7.2 ~ 115.0 mg) CGA were added to 10.0 mL of 1 M $ZnSO_4$ solution to prepare CGA/$ZnSO_4$ electrolytes at different concentrations. All prepared electrolytes are kept at room temperature without light.

3) Cell assembly

Electrochemical performances were evaluated by CR-2032 coin-type cells, using pure 1 M $ZnSO_4$ or 1 M CGA/$ZnSO_4$ as the electrolyte, and glass fiber as the separator. The electrolyte volume is 120.0 μL in one coin cell. Zn//Zn symmetric cells were assembled by using two bare Zn foils (1 cm^2). Zn//Cu asymmetric cells were assembled by using bare Cu foil as the working electrode and Zn foil as the counter electrode. Full cells were assembled by using a MnO_2 electrode as the cathode and bare Zn foil as the anode. All cells are tested immediately after assembly, unless otherwise specified.

4) Material characterization

The X-ray diffraction (XRD) patterns were collected on a German Bruker (D8 Advance) with Cu Kα radiation. The morphologies of the Zn metal were confirmed by scanning electron microscope (SEM). The deposition behavior of Zn^{2+} ions on Zn foil surfaces in different electrolytes was observed by optical microscopy in a homemade symmetric cell tester. The solvation structures of Zn^{2+} ions in various solutions were studied by Fourier-transform infrared spectroscopy (FTIR, Nicolet 6700). Raman spectroscopy analysis of the modified and unmodified electrolytes was performed using a Raman microscope system (LabRam HR Evolution). Laser confocal microscopy was used to observe the 3D reconstructed morphology of the Zn metal surface after cycling.

5) Electrochemical measurements

The assembled Zn//Zn symmetric cells, Zn//Cu asymmetric cells, and Zn//MnO_2 full cells were tested on a battery test system (LAND CT3002A) for long-term cycling performance.

Other electrochemical data was tested using a CHI760E electrochemical workstation from Wuhan Corrtest Instruments Corp. In detail, the hydrogen evolution reactions (HER) of a two-electrode system, with a Zn plate as the reference electrode and working electrode, was investigated via linear sweep voltammetry (LSV) at a scanning rate of 5 mV s^{-1} within the range of 0 to -0.4 V. Furthermore, these plots were obtained at a duration of 3600 s. The Tafel plot test involved a two-electrode system with a scanning rate of 1 mV s^{-1}. The CV curves of the Zn//Cu asymmetric cells were recorded between -0.2 V and 0.4 V at a scanning rate of 0.5 mV s^{-1}. Noteworthy, Zn//Zn symmetrical batteries were placed in a high and low-temperature chamber to test EIS spectra at different temperatures (40 ~ 90°C) over a frequency range of 10^5 to 1 Hz. The Zn//Cu asymmetric cells were cycled under various current densities with a charge cut-off voltage of 0.5 V, to get the coulombic efficiencies of Zn plating/stripping. Additionally, the electrochemical performance of the full cell was assessed through CV and GCD measurements, and the voltage windows for the full cells were 0.8 ~ 1.8 V. All electrochemical measurements were performed in the open air of a thermostatic room (25 ± 1 °C).

Calculation section

1) The density functional theory (DFT) calculations

The density functional theory (DFT) calculations were performed using CASTEP package with the Perdew-Burke-Ernzerhof (PBE) generalized gradient approximation (GGA) exchange-correlation functional. Interactions between core and valance electrons were described using Vanderbilt ultra-soft pseudopotentials. The energy cut-off for the plane-wave basis set was 340 eV was adopted. The threshold values of the convergence criteria were specified as follows: 0.002 Å for maximum displacement, 0.05 eV/Å for the maximum force, 0.1 GPa for the maximum stress, 10^{-5} eV/atom for energy, and 2.0×10^{-6} eV/atom for self-consistent field tolerance. The 1.5 Å thickness of Zn(002) surface was cleaved. 20 Å vacuum space were implemented into the model to eliminate undesirable interactions between bottom side of the slab and the molecules in the vacuum space.

2) The binding energy ($\Delta E_{binding}$) calculations

The binding energy ($\Delta E_{binding}$) was calculated as:

$$\Delta E_{binding} = E_{total} - (E_{vacancy} + E_{AA/EA/PA})$$

where the E_{total} is the energy of the optimized system; $E_{vacancy}$ is the energy of the vacancy structure; $E_{PZBGACl}$ is the energy of an optimized AA, EA and PA molecule within a 10 Å × 10 Å × 10 Å box.

3) Theoretical Calculation Methods

DFT calculations were carried out using the Gaussian 09 program. Geometries of intermediates and transition states were optimized using the dispersion-corrected B3LYP-D3 functional with basis set of Def2svp for all atoms.

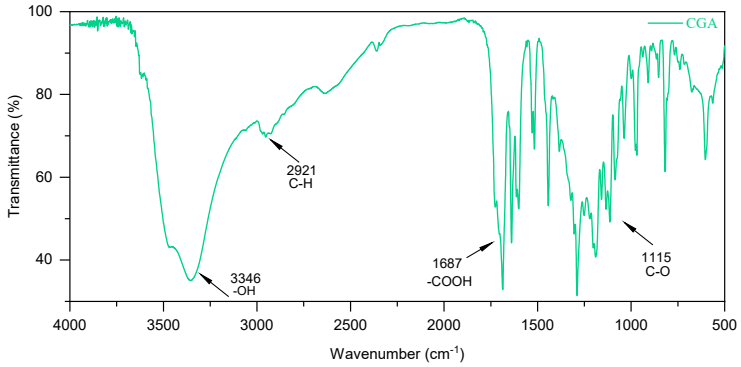

Figure S1. FTIR spectrum of CGA.

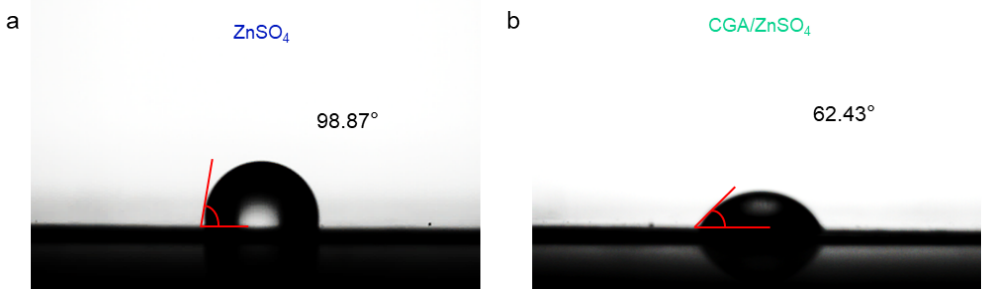

Figure S2. Contact angles of (a) $ZnSO_4$ and (b) $CGA/ZnSO_4$ electrolytes.

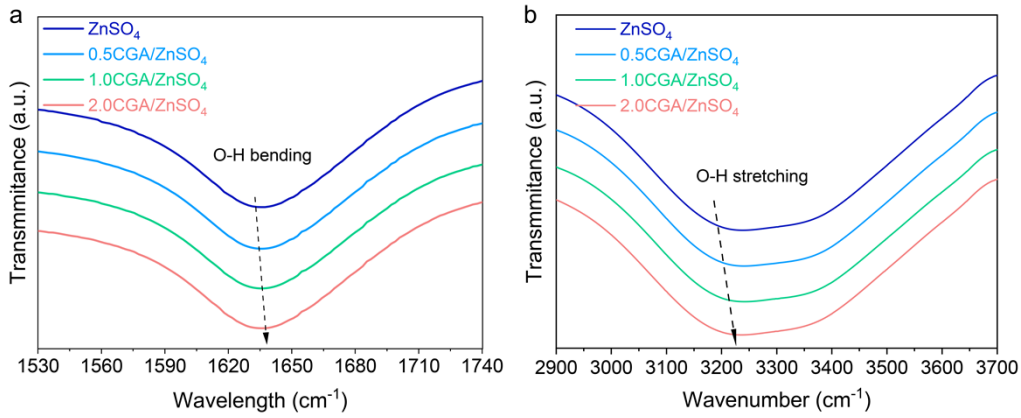

Figure S3. FTIR spectra of $ZnSO_4$ electrolyte with different ratios of CGA: (a) O-H bending and (b) O-H stretching.

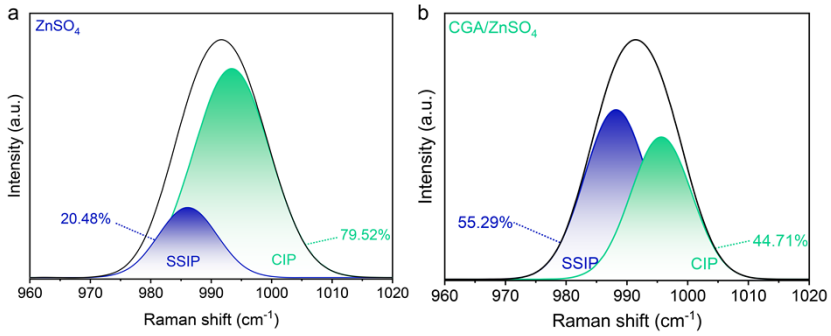

Figure S4. Raman spectra of *v*-SO_4^{2-} for (a) $ZnSO_4$ and (b) $CGA/ZnSO_4$ electrolytes.

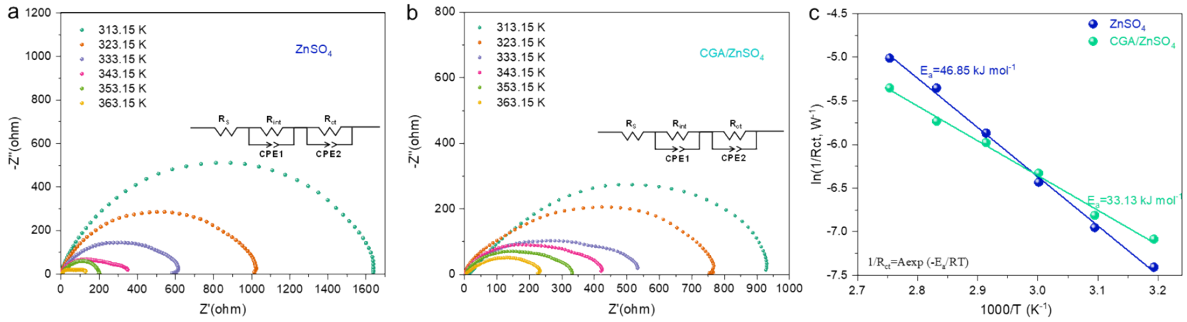

Figure S5. Nyquist plots of Zn//Zn symmetric cells under varying temperature conditions in (a) $ZnSO_4$ and (b) $CGA/ZnSO_4$ electrolytes. (c) Arrhenius behavior of temperature-dependent reciprocal resistances of Zn metal anode in $ZnSO_4$ and $CGA/ZnSO_4$ electrolytes.

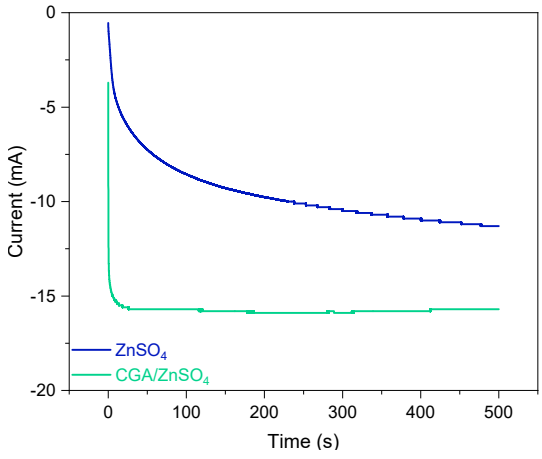

Figure S6. CA results of Zn//Zn symmetrical cells in $ZnSO_4$ and $CGA/ZnSO_4$ electrolytes.

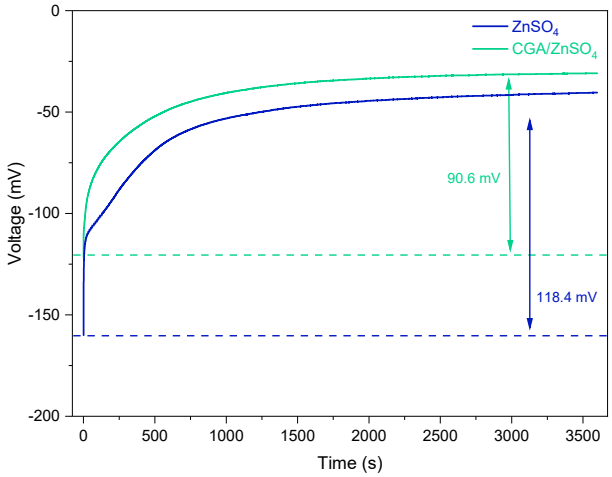

Figure S7. Initial Zn nucleation overpotential of Zn//Zn symmetric cells in $ZnSO_4$ and $CGA/ZnSO_4$ electrolytes.

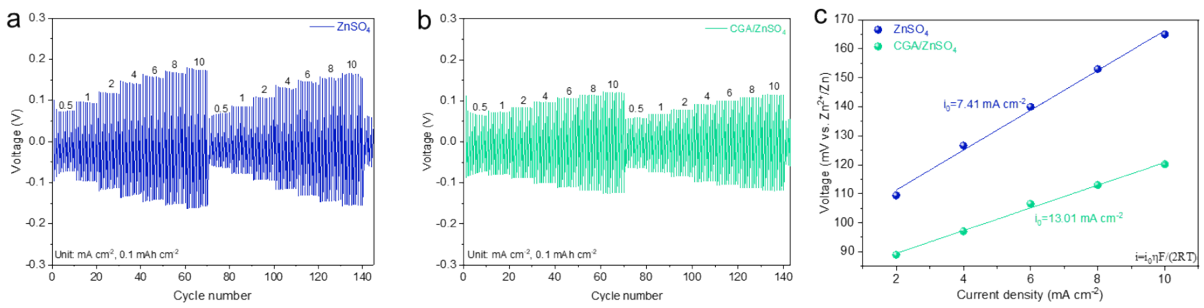

Figure S8. Rate performance of Zn//Zn symmetric cells during Zn stripping/plating at different current densities from 0.5 to 10 mA cm^{-2} with the capacity of 0.1 mAh cm^{-2} in (a) $ZnSO_4$ and (b) $CGA/ZnSO_4$ electrolytes. (c) The exchange current densities at different cycle numbers in $ZnSO_4$ and $CGA/ZnSO_4$ electrolytes.

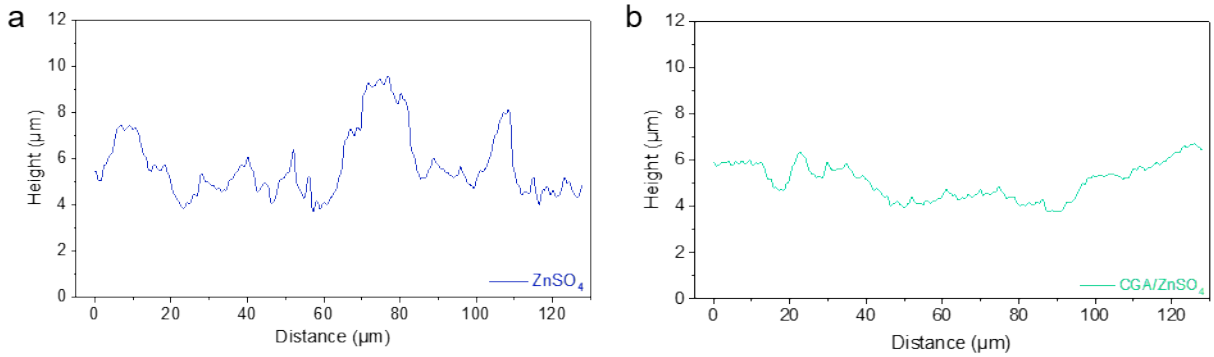

Figure S9. Height profile line of Zn metal anode after 15 cycles under 1 mA cm^{-2}/1 mAh cm^{-2} in (a) $ZnSO_4$ and (b) $CGA/ZnSO_4$ electrolytes.

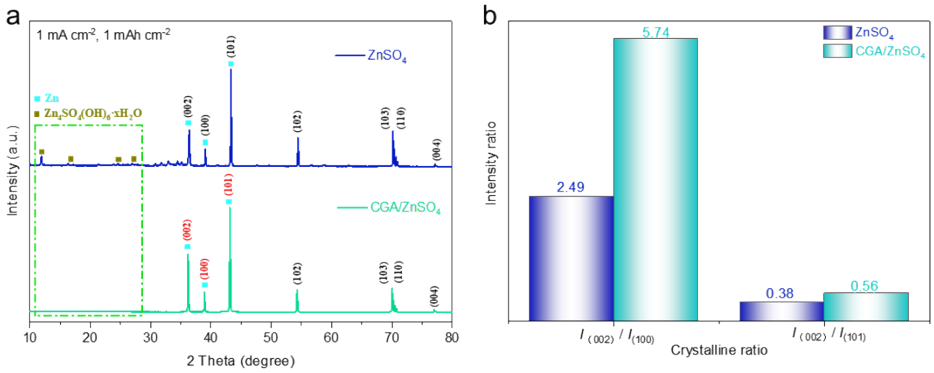

Figure S10. (a) XRD patterns of cycled Zn metal anode in $ZnSO_4$ and $CGA/ZnSO_4$ electrolytes at 1 mA cm^{-2} and 1 mAh cm^{-2} for 100 h. (b) Intensity ratios of the (002) crystal plane to (101) and (100) crystal plane of the Zn metal anode in $ZnSO_4$ and $CGA/ZnSO_4$ electrolytes.

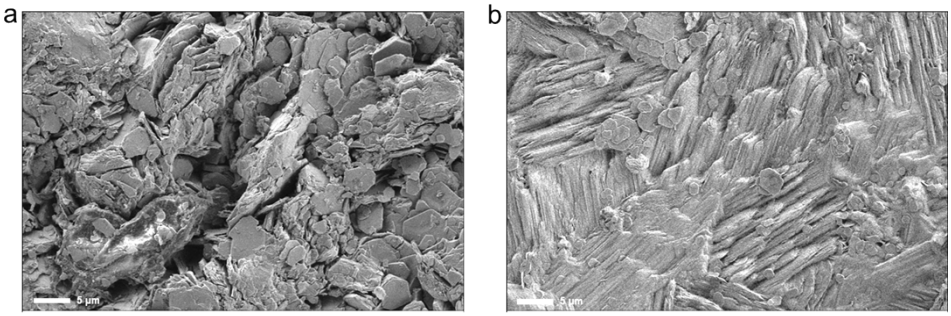

Figure S11. SEM images of cycled Zn metal anodes in (a) $ZnSO_4$ and (b) $CGA/ZnSO_4$ electrolytes at 1 mA cm^{-2} and 1 mAh cm^{-2} for 100 h.

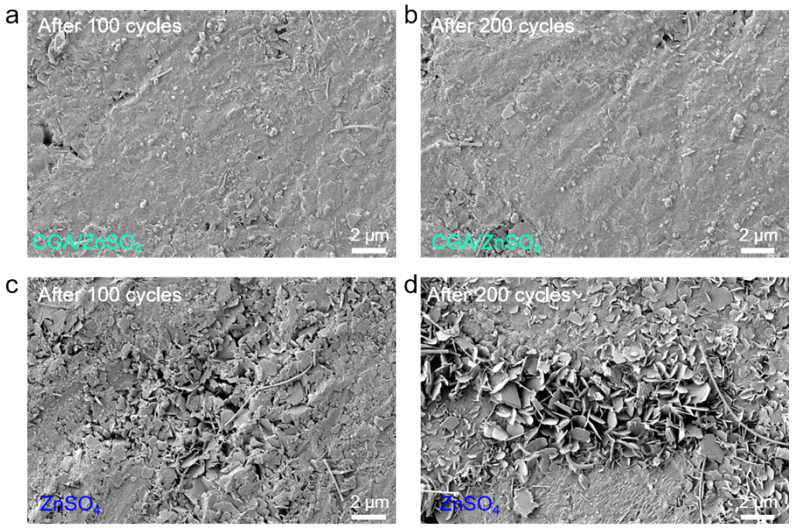

Figure S12. SEM images of cycled Zn anodes in $CGA/ZnSO_4$ electrolyte for (a) 100, (b) 200 cycles and in $ZnSO_4$ electrolyte for (c) 100, (d) 200 cycles at 5 mA cm^{-2}/1 mAh cm^{-2}.

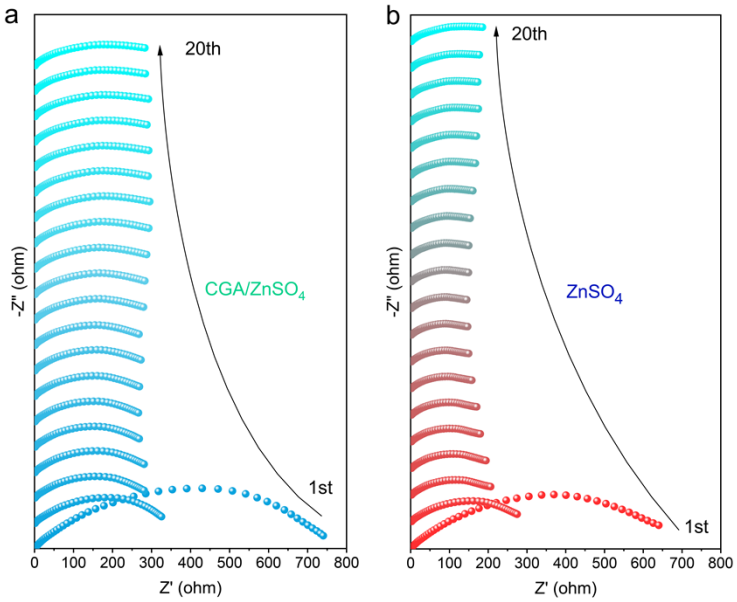

Figure S13. *In-situ* EIS of Zn//Zn symmetric cells with (a) $CGA/ZnSO_4$ and (b) $ZnSO_4$ electrolytes cycled at 1 mA cm^{-2} and 1 mAh cm^{-2} for 20 cycles.

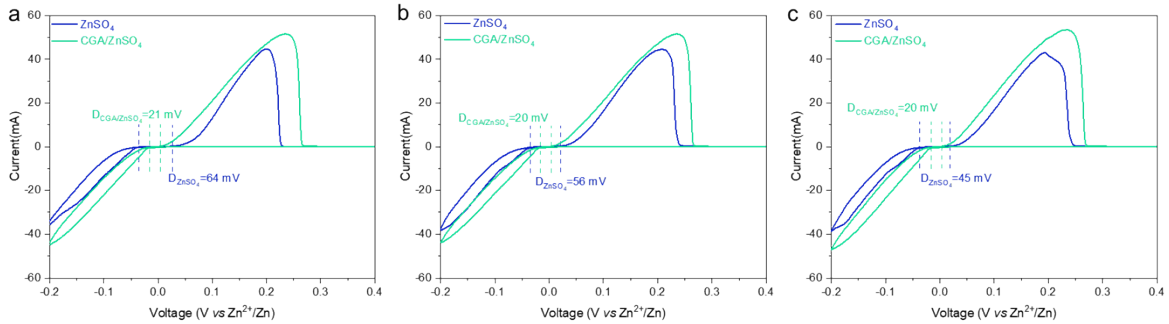

Figure S14. CV curves for Zn plating/stripping of Zn//Cu asymmetric cells in $ZnSO_4$ and $CGA/ZnSO_4$ electrolytes at (a) 1st, (b) 10th, (c) 20th cycles.

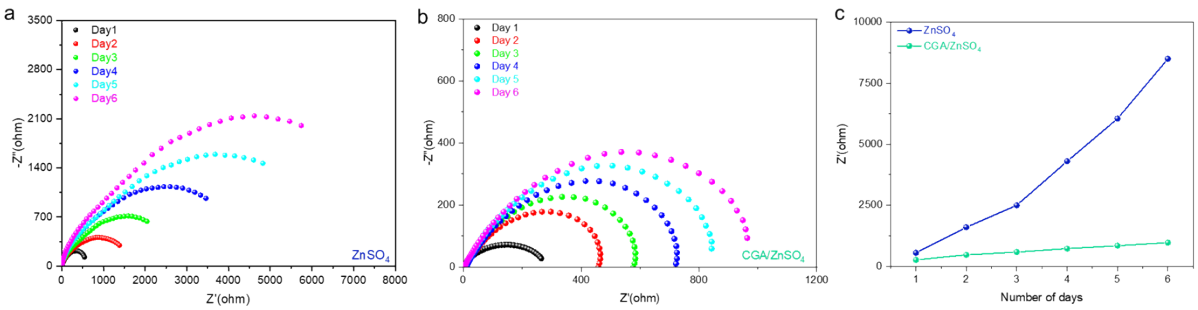

Figure S15. EIS of the Zn//Zn symmetric cells at different days in (a) $ZnSO_4$ and (b) $CGA/ZnSO_4$ electrolytes and (c) their comparison.

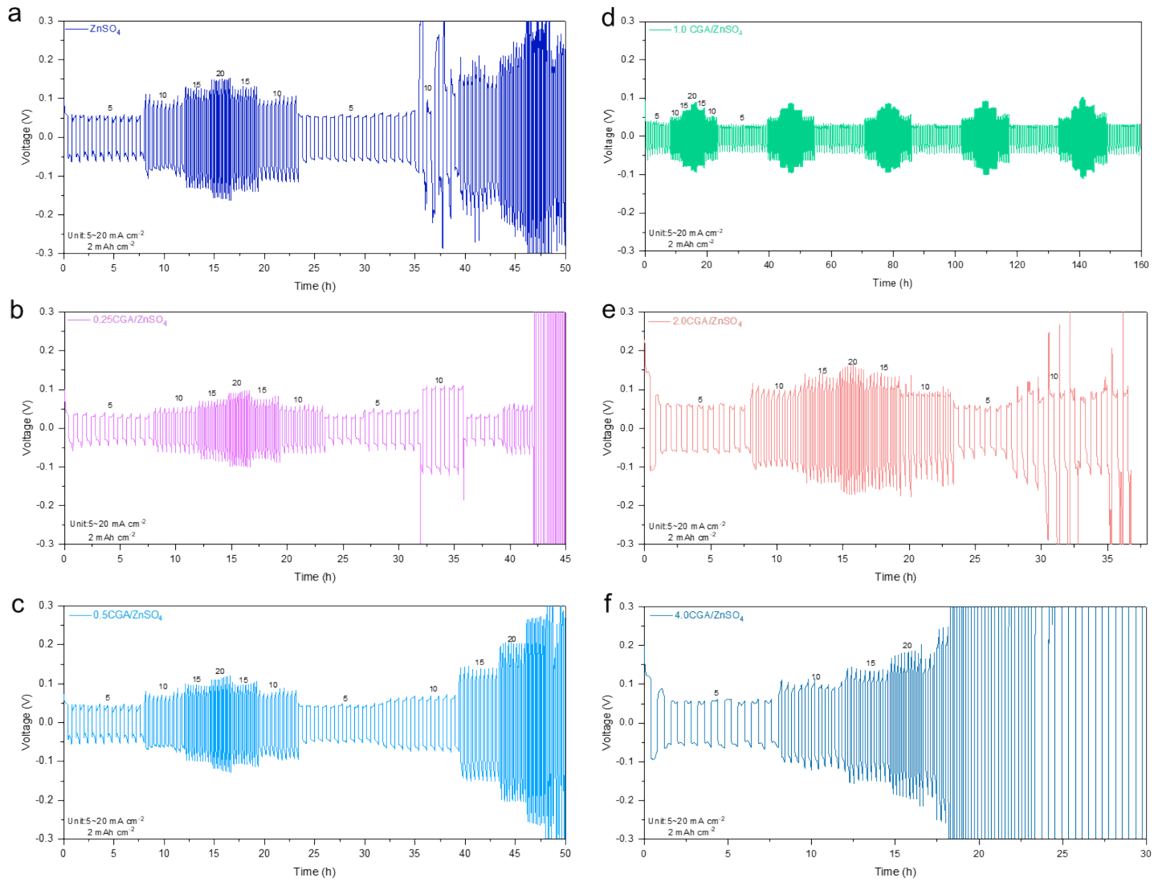

Figure S16. Rate performance of Zn//Zn symmetric cells during Zn plating/stripping at different current densities from 5 to 20 mA cm^{-2} with the capacity of 2 mAh cm^{-2} in (a) $ZnSO_4$, (b) 0.25CGA/$ZnSO_4$, (c) 0.5CGA/$ZnSO_4$, (d) 1.0CGA/$ZnSO_4$, (e) 2.0CGA/$ZnSO_4$, and (f) 4.0CGA/$ZnSO_4$ electrolytes.

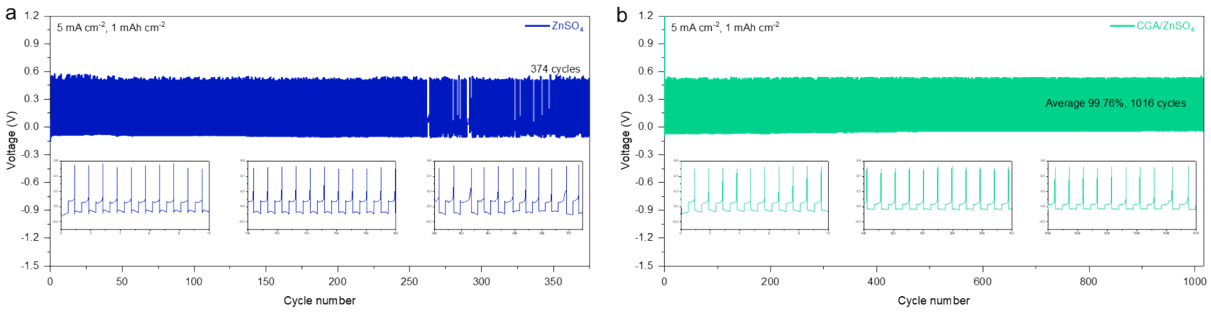

Figure S17. Charge/discharge curves of Zn//Cu asymmetric cells at 5 mA cm^{-2} with 1 mAh cm^{-2} in (a) $ZnSO_4$ and (b) CGA/$ZnSO_4$ electrolytes.

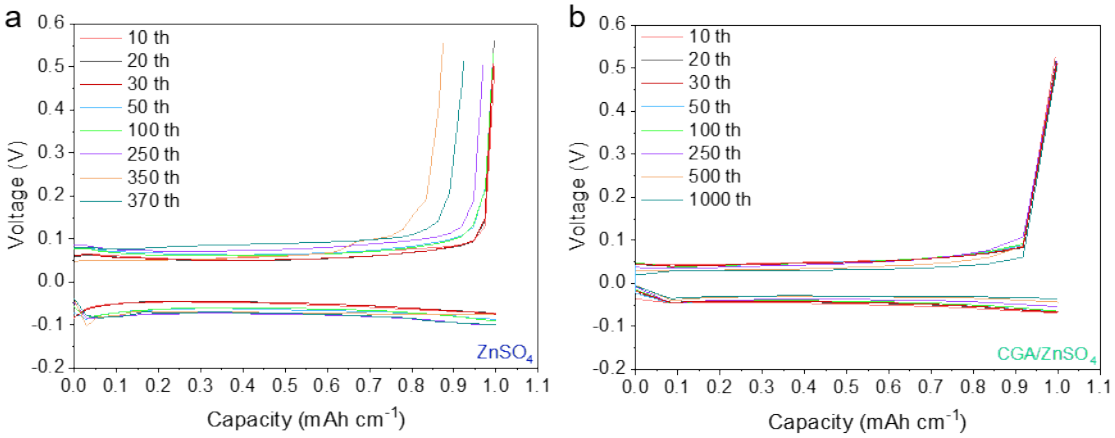

Figure S18. Capacity-voltage curves of Zn//Cu asymmetric cells at the selected cycles at 5 mA cm^{-2} with 1 mAh cm^{-2} in (a) $ZnSO_4$ and (b) $CGA/ZnSO_4$ electrolytes.

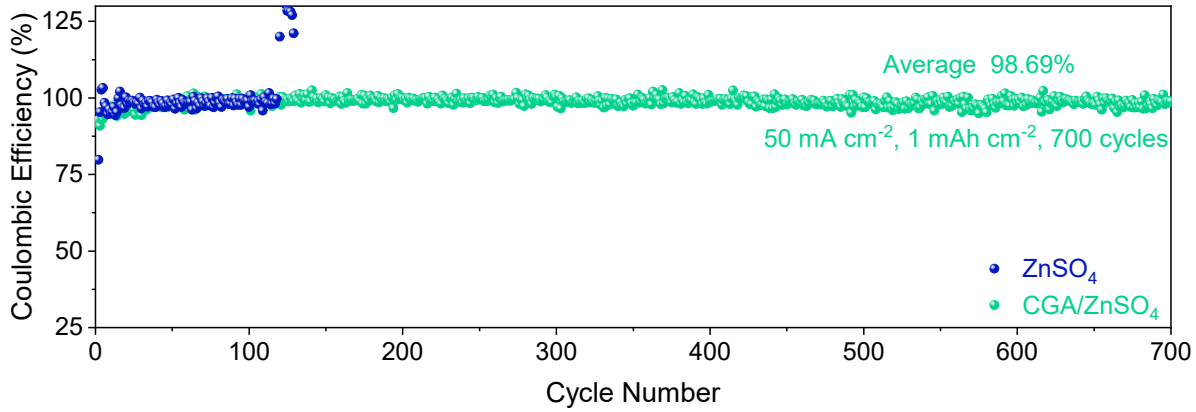

Figure S19. Comparison of Zn plating/stripping efficiency at 50 mA cm^{-2} with 1 mAh cm^{-2} in Zn//Cu asymmetric cells in $ZnSO_4$ and $CGA/ZnSO_4$ electrolytes.

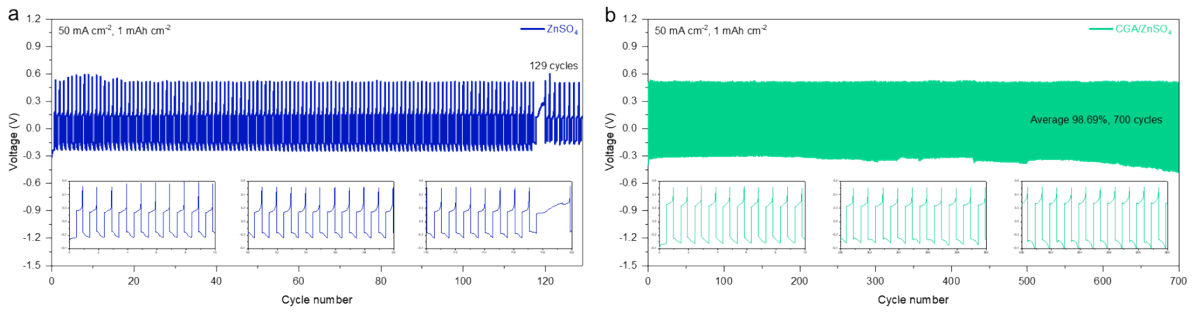

Figure S20. Charge/discharge curves of Zn//Cu asymmetric cells at 50 mA cm^{-2} with 1 mAh cm^{-2} in (a) $ZnSO_4$ and (b) $CGA/ZnSO_4$ electrolytes.

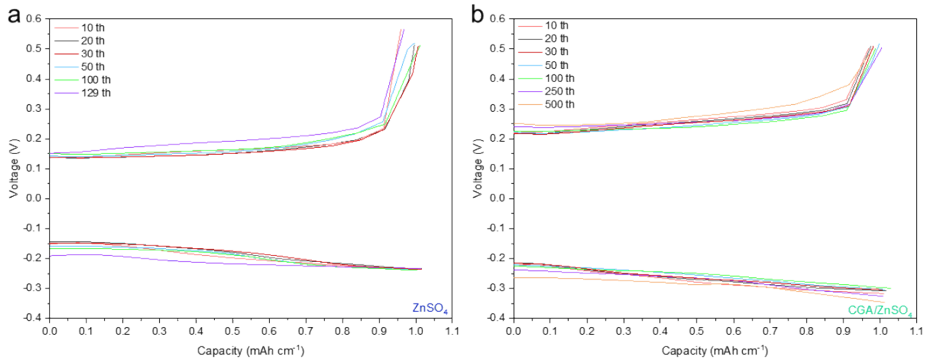

Figure S21. Capacity-voltage curves of Zn//Cu asymmetric cells at the selected cycles at 50 mA cm^{-2} with 1 mAh cm^{-2} in (a) $ZnSO_4$ and (b) CGA/$ZnSO_4$ electrolytes.

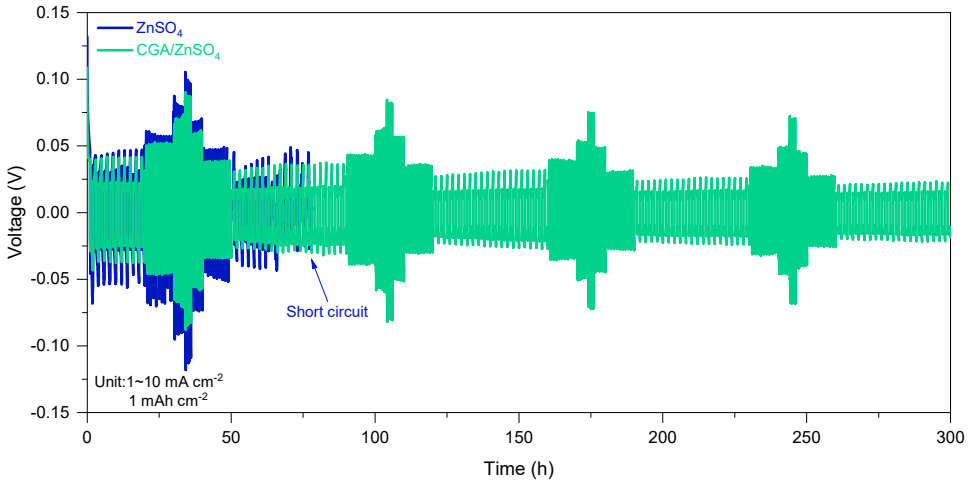

Figure S22. Rate performance of Zn//Zn symmetric cells during Zn plating/stripping at different current densities from 1 to 10 mA cm^{-2} with the capacity of 1 mAh cm^{-2} in $ZnSO_4$ and CGA/$ZnSO_4$ electrolytes.

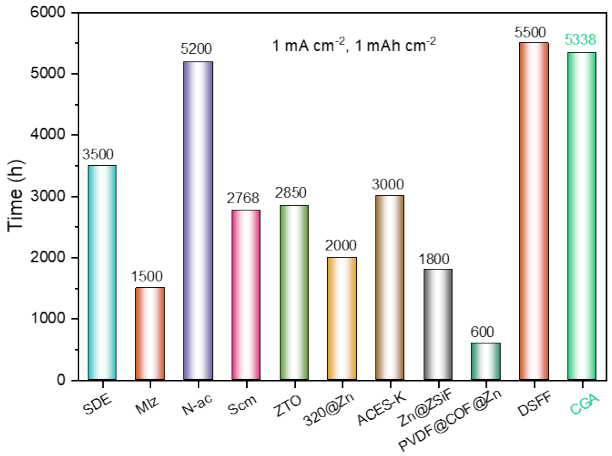

Figure S23. Performance comparison of Zn//Zn symmetric cells cycled at 1 mA cm^{-2} and 1 mAh cm^{-2} in this work with the previously reported works.

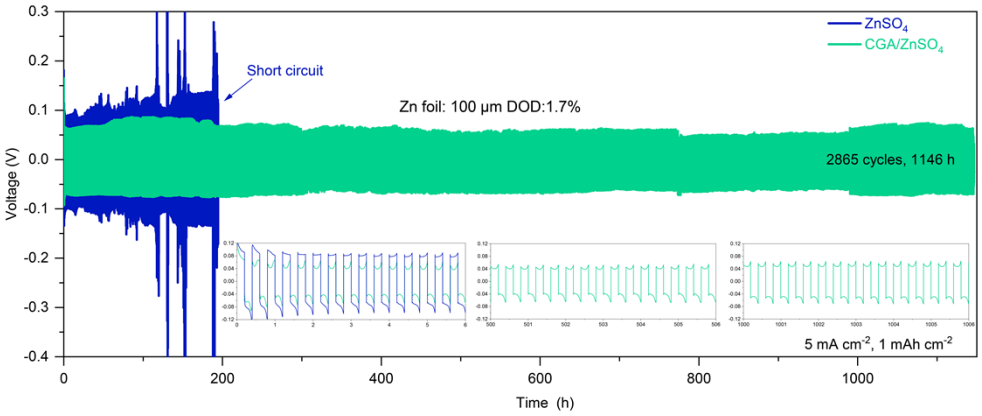

Figure S24. Long-term cycling performance of Zn//Zn symmetric cells at 5 mA cm^{-2} with the plating/stripping capacity of 1 mAh cm^{-2} in $ZnSO_4$ and $CGA/ZnSO_4$ electrolytes.

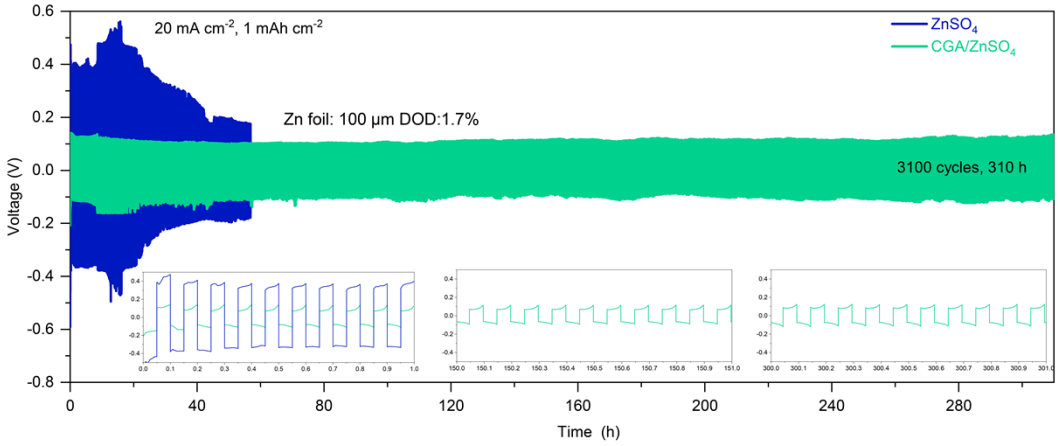

Figure S25. Long-term cycling performance of Zn//Zn symmetric cells at 20 mA cm^{-2} with the plating/stripping capacity of 1 mAh cm^{-2} in $ZnSO_4$ and $CGA/ZnSO_4$ electrolytes.

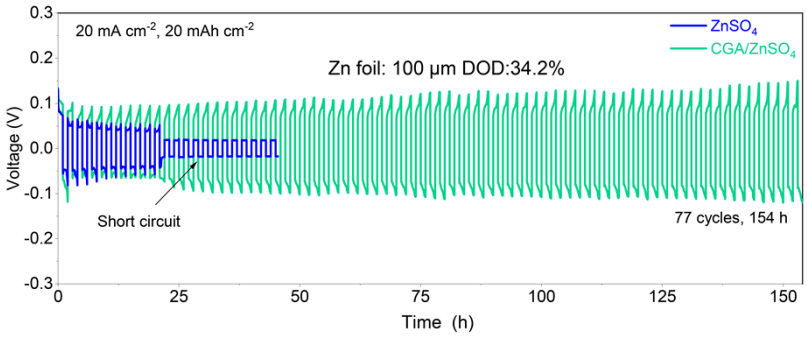

Figure S26. Long-term cycling performance of Zn//Zn symmetric cells at 20 mA cm^{-2} with the plating/stripping capacity of 20 mAh cm^{-2} in $ZnSO_4$ and $CGA/ZnSO_4$ electrolytes.

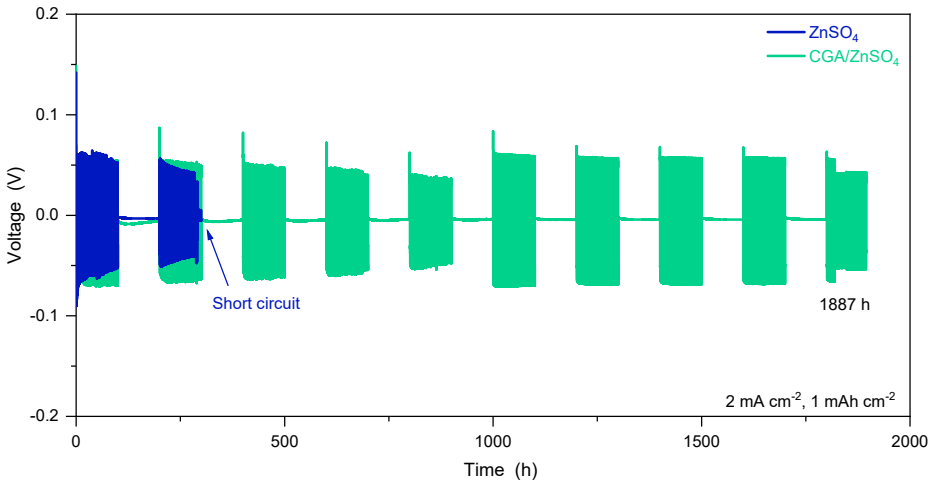

Figure S27. The shelving-recovery performances of Zn//Zn symmetric cells at 2 mA cm^{-2} and 1 mAh cm^{-2} in $ZnSO_4$ and $CGA/ZnSO_4$ electrolytes.

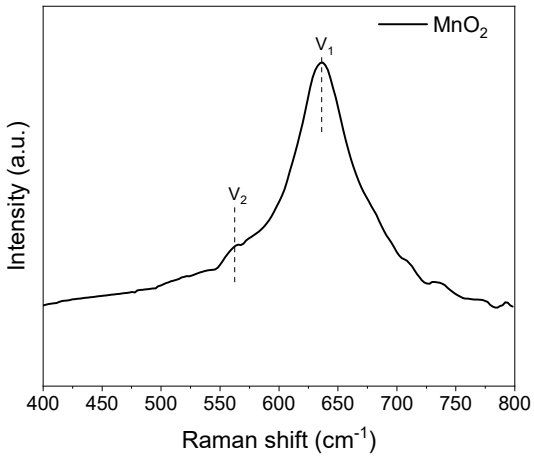

Figure S28. Raman spectra of the MnO_2 electrode.

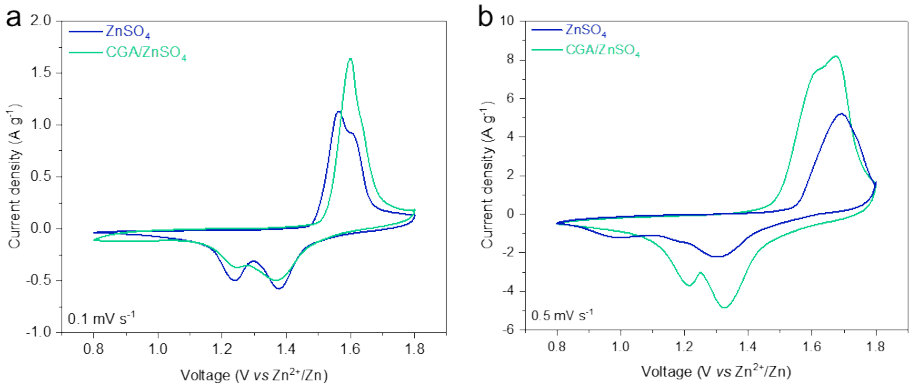

Figure S29. CV curves of full cells using MnO_2 as cathode and Zn foil as anode in $ZnSO_4$ and $CGA/ZnSO_4$ electrolytes at (a) 0.1 mV s^{-1} and (a) 0.5 mV s^{-1}.

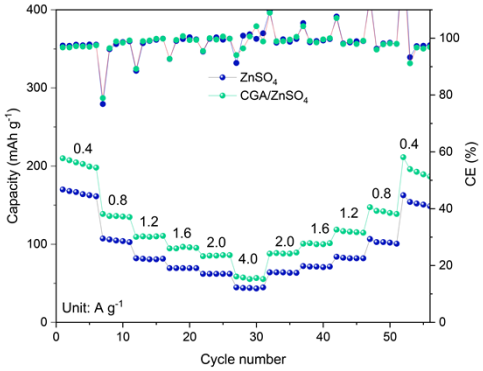

Figure S30. Rate capabilities and CE of Zn//MnO_2 full cells.

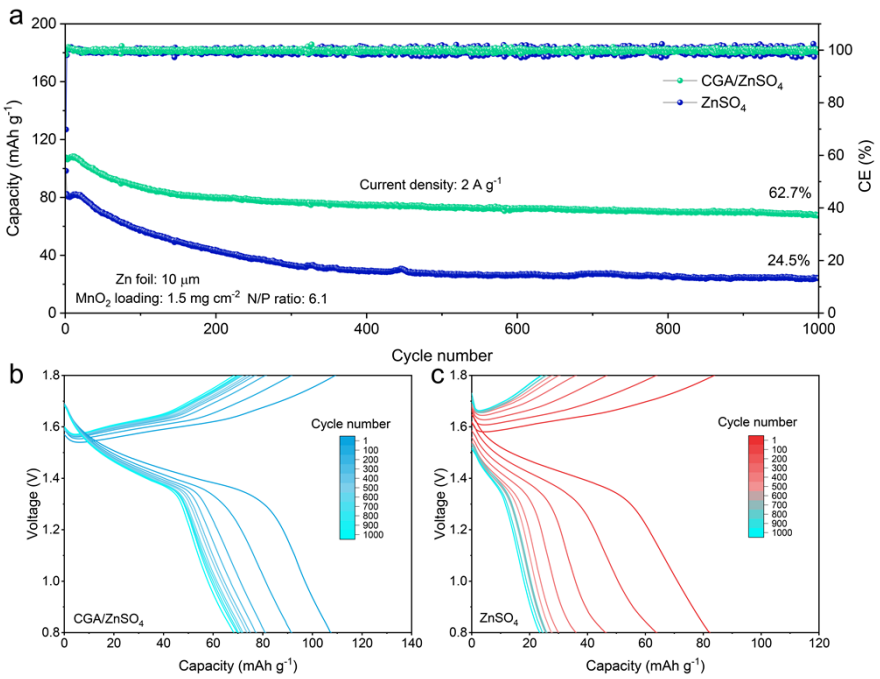

Figure S31. (a) Capacity retentions and corresponding charge/discharge voltage profiles of Zn//MnO_2 full cells with (b) CGA/$ZnSO_4$ and (c) $ZnSO_4$ electrolytes.

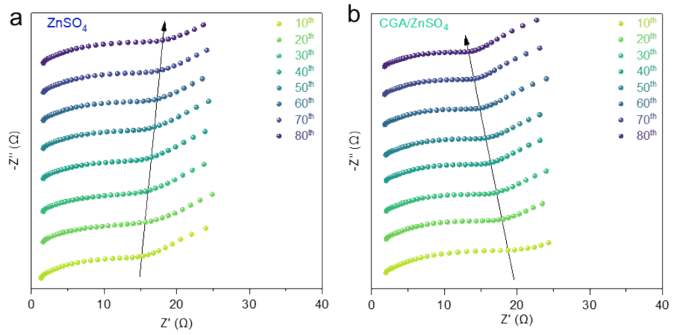

Figure S32. *In situ* EIS curves of full cells at different cycle numbers in (a) $ZnSO_4$ and (b) CGA/$ZnSO_4$ electrolytes.

Table S1. Performance comparison of Zn//Zn symmetric cells cycled at 1 mA cm^{-2} and 1 mAh cm^{-2} in this work with the previously reported works. The complete designations for the abbreviations listed under the "Additive", "Protective layer" and "Co-solvent electrolyte" column are 2, 2'-Sulfonyldiethanol (SDE)[1], 2-methylimidazole (MIz)[2], N-Acetyl-ε-caprolactam (N-ac)[3], straight-chain molecule (Scm)[4], $ZnTiO_3$ (ZTO)[5], COF-320N (320N@Zn)[6], acesulfame potassium (ACES-K)[7], ammonium fluosilicate (ZSiF)[8], polyvinylidene fluoride @ covalent organic framework (PVDF@COF)[9], Dimethyl sulfoxide-trifluoroethyl formate (DSFF)[10].

Test condition	Modified type	Lifespan (h)	Ref.
1 mA cm^{-2}, 1 mAh cm^{-2}	**Additive** (SDE)[1]	3500	Angew. Chem. Int. Ed. 2024, **63**, e202411470
	Additive (MIz)[2]	1500	ACS Nano 2024, **18**, 16610
	Additive (N-ac)[3]	5200	Angew. Chem. Int. Ed. 2024, **63**, e202402833
	Additive (Scm)[4]	2768	Angew. Chem. Int. Ed. 2024, 10.1002/anie.202421787
	Protective layer (ZTO)[5]	2850	Adv. Energy Mater. 2025, 10.1002/aenm.202405804
	Protective layer (320N@Zn)[6]	2000	Angew. Chem. Int. Ed. 2025, 10.1002/anie.202424184
	Additive (ACES-K)[7]	3000	Angew. Chem. Int. Ed. 2025, 10.1002/anie.202422036
	Protective layer (Zn@ZSiF)[8]	1800	Angew. Chem. Int. Ed. 2025, 10.1002/anie.202423244
	Protective layer (PVDF@COF@Zn)[9]	600	Electrochim. Acta, 2024, 506, 145059
	Co-solvent electrolytes (DSFF)[10]	5500	Joule, 2025, 9, 101844
	Additive (Chlorogenic acid)	5340	*This work*

References

1 T. Yan, B. Wu, S. Liu, M. Tao, J. Liang, M. Li, C. Xiang, Z. Cui, L. Du, Z. Liang, H. Song, *Angew. Chem. Int. Ed.* 2024, **63**, e202411470

2 J. Cao, M. Sun, D. Zhang, Y. Zhang, C. Yang, D. Luo, X. Yang, X. Zhang, J. Qin, B. Huang, Z. Zeng, J. Lu, *ACS Nano* 2024, **18**, 16610

3 D. Xu, X. Ren, H. Li, Y. Zhou, S. Chai, Y. Chen, H. Li, L. Bai, Z. Chang, A. Pan, H. Zhou, *Angew. Chem. Int. Ed.* 2024, **63**, e202402833

4 F. Wu, J. Zhang, L. Ma, P. Ruan, Y. Chen, S. Meng, R. Yin, W. Shi, W. Liu, J. Zhou, X. Cao, *Angew. Chem. Int. Ed.* 2024, **64**, e202421787

5 Y. Li, B. Ping, J. Qu, J. Ren, C. Lin, J. Lei, J. Chen, J. Li, R. Liu, X. Long, X. Guo, D. Luo, Z. Chen, *Adv. Energy Mater.* 2025, doi: 10.1002/aenm.202405804

6 S. Zhang, J. Chen, W. Chen, Y. Su, Q. Gou, R. Yuan, Z. Wang, K. Wang, W. Zhang, X. Hu, Z. Zhang, P. Wang, F. Wan, J. Liu, B. Li, Y. Wang, G. Zheng, M. Li, and J. Sun, *Angew. Chem. Int. Ed*. 2025, doi: 10.1002/anie.202424184

7 G. Qu, Y. Zhao, C. Li, Y. Zhai, Y. Kong, X. He, L. Kong, C. Wang, M. Chen, K. Song, Z. Liu, L. Xu, *Angew. Chem. Int. Ed.* 2025, doi: 10.1002/anie.202422036

8 G. Yin, H. Wang, M. Zhou, T. Long, M. Ding, B. Xie, X. Wu, J. Li, W. Ling, J. Dai, X. Zeng, *Angew. Chem. Int. Ed.* 2025, doi: 10.1002/anie.202423244

9 V. Aupama, J. Sangsawang, W. Kao-ian, S. Wannapaiboon, J. Pimoei, W. yoopensuk, M. Opchoei, Z. Tehrani, S. Margadonna, S. Kheawhom, *Electrochemica Acta.* 2024, **506**, 145059

10 J. Heo, D. Dong, Z. Wang, F. Chen, C. Wang, Joule **9**, 101844